Biomaterials Science

ROYAL SOCIETY OF CHEMISTRY

PAPER

View Article Online
View Journal | View Issue

Cite this: *Biomater. Sci.*, 2020, **8**, 6350

Silver-decorated, light-activatable polymeric antimicrobials for combined chemo-photodynamic therapy of drug-resistant bacterial infection†

Xiaoxue Hou,‡ Lijun Yang,‡ Jinjian Liu, Yumin Zhang, Liping Chu, Chunyan Ren, Fan Huang* and Jianfeng Liu *

Drug-resistant bacterial infections have stolen the spotlight in recent years as stubborn diseases intimidating public health, thus urgently requiring the development of innovative treatment strategies with high antibacterial efficiency and low bacterial resistance. Here, a polymeric antimicrobial with synergistic chemo-photodynamic therapy function is fabricated to combat drug-resistant bacterial infections. In this strategy, polymeric micelles based on amphiphilic poly(aspartic acid)-*block*-poly(ε-caprolactone) (PAsp-*b*-PCL) are used as nanocarriers to encapsulate a photosensitizer protoporphyrin IX (PpIX) in the micellar core, which then undergo silver nanoparticle decoration on the micellar shell through an *in situ* reduction method. Compared with mono-therapy, the combination of silver nanoparticle decoration and light-activatable PpIX enables the resulting polymeric antimicrobial to exert chemo-photodynamic activity to kill drug-resistant bacteria more potently *in vitro*. Furthermore, the prepared polymeric antimicrobials with synergistic antibacterial activity show robust eradication efficacy against subcutaneous infections induced by drug-resistant *Staphylococcus aureus* in a murine model. Therefore, our study provides a simple and potent strategy to realize combination therapy for eradicating drug-resistant bacterial infections.

Received 2nd July 2020,
Accepted 10th September 2020

DOI: 10.1039/d0bm01084g

rsc.li/biomaterials-science

Introduction

In recent years, bacterial infections have become a serious threat to public health across the globe.[1,2] The rate of emergence and transmission of antibiotic-resistant bacteria alarmingly increased apparently due to the abuse of antibiotics.[3,4] Despite extensive efforts having been made for the development of novel antibiotics, it still cannot catch up with the evolution and spread rate of drug-resistant bacteria.[5,6] Thus, researchers in an increasing number have focused on exploring alternative methods to combat drug-resistant bacterial infections.[7–9] Various antibacterial methods such as inhibition of bacterial adhesion,[10] photothermal bacteria killing,[11,12] photocatalytic bacteria killing,[13,14] synergistic bacteria killing,[15] *etc*. have emerged. Moreover, a multitude of research has shown that photodynamic therapy (PDT) is a promising strategy to fight against bacterial infections because of its lesser trauma, higher selectivity, smaller side effects and capability of avoiding the production of bacterial resistance.[16–18] Typically, upon excitation at specific wavelengths, PDT could convert molecular oxygen into reactive oxygen species (ROS) through a light-activated photosensitizer (PS),[19–21] leading to the destruction of bacteria by interacting with biological macromolecules such as proteins, DNA and phospholipids. Therefore, an effective PS producing a high concentration of ROS plays an essential role in PDT with respect to bacterial infections. Protoporphyrin IX (PpIX), a key precursor of biomolecules such as chlorophyll, heme and cytochrome, has become a promising PS because of its excellent photophysical properties.[22,23] However, the ROS production efficiency of PpIX dramatically decreases due to its low water solubility and aggregation in the physiological environment, which directly limits its application for PDT.[24,25] Hitherto, in order to improve the PDT performance of PpIX, various nanoscale materials including gold nanoparticles,[26] silica nanoparticles,[27] upconversion nanoparticles,[28] and polymeric structures[29,30] have been widely studied to resist PpIX aggregation and optimize their ROS-producing efficiency. However, in many cases, monotherapy could not completely eradicate bacterial infections, especially complicated drug-resistant bac-

Tianjin Key Laboratory of Radiation Medicine and Molecular Nuclear Medicine, Institute of Radiation Medicine, Chinese Academy of Medical Science & Peking Union Medical College, Tianjin 300192, P. R. China. E-mail: huangfan@irm-cams.ac.cn, liujianfeng@irm-cams.ac.cn

†Electronic supplementary information (ESI) available. See DOI: 10.1039/d0bm01084g

‡These authors contributed equally to this work.

teria. Therefore, it is imperative to develop a facile combination therapy with high curative efficacy and low resistance for combating drug-resistant bacterial infections.[31,32]

The *de novo* designed antimicrobial agents such as copper-based,[33,34] xerogel materials,[35] silica-based,[36] silver nanoparticles,[37] *etc*. have been extensively investigated to date. Among them, silver nanoparticles as a kind of commercialized nanomaterial used in the medical field and consumer products have been applied as an excellent antibacterial agent due to their broad-spectrum antimicrobial activity, less bacterial resistance and slight toxicity.[38,39] Silver nanoparticles can easily enter the cytoplasm of bacterial cells through destroying the bacterial membrane. They can further interact with intracellular proteins and DNA to cause bacterial apoptosis and exert their antibacterial activity by releasing silver ions.[40,41] Therefore, combining silver nanoparticles with PDT would be an attractive strategy for bacterial inactivation with enhanced efficiency.[42,43] Nevertheless, silver nanoparticles usually form agglomerates because of their small size, which will result in a significant reduction of antibacterial activity.[44,45] For conquering this limitation, silver nanoparticles were frequently supported with other materials such as regenerated cellulose membranes,[46] gold nanoparticles,[47] hollow CeO_2 nanocontainers,[48] graphene oxide,[49] and polymeric structures.[50] Among them, polymeric micelles have been proved to be commendable templates for stabilizing silver nanoparticles and preventing their unfavorable aggregation, benefiting from their flexible compositions and easy preparation. Furthermore, polymeric micelles are capable of simultaneously delivering different drugs to exert multiple functions. Thus, it is highly desirable to integrate silver nanoparticles and PDT within a simple polymeric micelle to make full use of their synergistic antibacterial effect.

Herein, we developed a facile silver-decorated, light-activatable polymeric antimicrobial for combined chemo-photodynamic therapy of bacterial infections. In our approach (Scheme 1), an amphiphilic diblock copolymer poly(aspartic acid)-*block*-poly(ε-caprolactone) (PAsp-*b*-PCL) and photosensitizer PpIX can self-assemble into polymeric micelles in aqueous solution, in which the shell consists of hydrophilic PAsp and the core consists of hydrophobic PCL and PpIX. Due to the abundant carboxyl groups and negative charges in the shell, the as-prepared polymeric micelle (PM@PpIX) can offer large available binding sites and electrostatic interactions for Ag^+ ions, which are easily *in situ* reduced into silver nanoparticles once a reductive agent is added and thus the novel combination strategy of concurrently decorating silver nanoparticles and encapsulating PpIX (PM@PpIX@Ag) is achieved. After having reached the infection sites, the resulting polymeric antimicrobial can attach to the bacteria and damage the bacterial membrane to some extent through the silver nanoparticles modifying the micellar shell. Moreover, upon light irradiation, the photosensitivity of PpIX in the micellar core will be activated and it generates ROS *in situ* to further inactivate bacteria, thus enhancing the eradication efficiency for persistent bacterial infection. Furthermore, due to the strong synergistic antibacterial effect, this polymeric antimicrobial with combined chemo-photodynamic activity was also successfully applied for the treatment of drug-resistant bacterial subcutaneous infections on a mouse model.

Materials and methods

Materials

ε-Caprolactone (ε-CL, 99%), stannous octoate ($Sn(Oct)_2$, 96%), and trifluoromethanesulfonic acid (CF_3SO_3H, 98%) were purchased from Shanghai Aladdin Biochemical Technology Co., Ltd. β-Benzyl L-aspartate-*N*-carboxyanhydride (BLA-NCA), trifluoroacetic acid (TFA, 98%), trifluoromethanesulfonic acid (CF_3SO_3H, 98%), trimethylamine (TEA, 99%), and silver nitrate ($AgNO_3$, 99.9%) were obtained from Alfa Asear and used as received. Protoporphyrin IX, sodium borohydride ($NaBH_4$, 98%), and tBoc-aminoethyl alcohol (99%) were purchased from Sigma-Aldrich Chemical Company. All the organic solvents were redistilled prior to use. Ultrapure Milli-Q water (re-

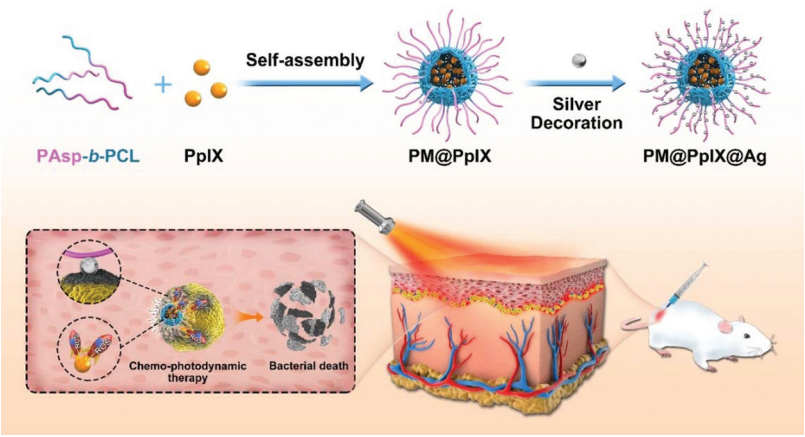

Scheme 1 Schematic illustration of the fabrication of the silver-decorated, light-activatable polymeric antimicrobials for the eradication of bacterial infection.

sistance >18 MΩ cm^{-1}) was used to make all aqueous solutions.

Preparation of the block copolymers

The synthetic process of PAsp-*b*-PCL was consistent with previous reports.[2] First, the ε-CL monomer in refluxed toluene was used to prepare the PCL-NHBoc by ring-opening polymerization (ROP) with an initiator *t*-Boc-aminoethyl alcohol and a catalyst $Sn(Oct)_2$. In a word, *t*-Boc-aminoethyl alcohol (0.32 g, 2 mmol), ε-CL (20.0 g, 175.6 mmol) and a drop of $Sn(Oct)_2$ were successively added into a clean Schlenk flask with 20 mL of anhydrous toluene. The reaction solution under a dry argon atmosphere (after three successive cycles of freezing, pumping and thawing) was stirred at 110 °C for 12 h. The reaction solution was then added to a micro amount of dichloromethane to dilute and a precipitant was formed by the action of excess diethyl ether. The intermediate PCL-NHBoc was successfully prepared *via* filtering and drying the precipitate.

The PCL-NH_2 macroinitiator was prepared through removing the Boc group of PCL-NHBoc. Briefly, the PCL-NHBoc dissolved in trifluoroacetic acid/dichloromethane solution was stirred for 12 h at 20 °C, and formed precipitates through superfluous diethyl ether, which were separated *via* screening. Then, the sediment was treated with dichloromethane/trimethylamine solution and the intermediate PCL-NH_2 was prepared through repeating the above procedures.

For the synthesis of PCL-*b*-PAsp, the benzyl groups of poly(ε-caprolactone)-*block*-poly(β-benzyl-L-aspartate) (PCL-*b*-PBLA) were removed by the ROP of β-benzyl-L-aspartate-*N*-carboxyanhydride (BLA-NCA) under the action of PCL-NH_2. Commercially available BLA-NCA (5.0 g, 20 mmol) and as-prepared PCL-NH_2 (4.0 g, 0.4 mmol) were added in 30 mL of dichloromethane. The reaction solution was stirred for 24 h at 30 °C and precipitated into excessive diethyl ether. PCL-*b*-PBLA was prepared through filtering and vacuum drying. Furthermore, 2.0 g of PCL-*b*-PBLA was dissolved in trifluoroacetic acid/trifluoromethanesulfonic acid/anisole solution for the removal of the benzyl group. The mixture was stirred for 2 h in an ice-water bath and added to a micro amount of dichloromethane to form the precipitant PCL-*b*-PAsp.

Synthesis of different polymeric antimicrobials

To synthesize the polymeric micelles (PM), PCL-*b*-PAsp solution (in anhydrous DMF) at 5.0 mg mL^{-1} was added drop by drop into nine times the volume of phosphate buffer (1 mM, pH 7.4) to form stable micelles after stirring for 4 h at room temperature. The solutions were dialyzed against ultrapure water using a dialysis bag to completely remove DMF.

For the preparation of protoporphyrin IX-loaded polymeric micelles (PM@PpIX), 1.0 mg of protoporphyrin IX was dissolved in the polymer solution and the resulting mixture was added drop by drop into nine times the volume of phosphate buffer (1 mM, pH 7.4), following the same steps as described in detail above.

Silver-decorated polymeric micelles (PM@Ag) were obtained by the following method. 100 μL of $AgNO_3$ solution (5 mg mL^{-1}) was added dropwise in the PM solution under magnetic stirring at 0 °C in the dark. 50 μL of freshly prepared $NaBH_4$ solution (30 mg mL^{-1}) was then rapidly mixed and the appearance of the brown solution turned yellow immediately. The solution was then stirred for 4 h in the dark and was then dialyzed against ultrapure water using a dialysis bag to prepare PM@Ag.

As for protoporphyrin IX-loaded Ag micelles (PM@PpIX@Ag), 100 μL of $AgNO_3$ solution (5 mg mL^{-1}) was added to PM@PpIX solution under magnetic stirring for 4 h at 25 °C in the dark, following the same steps as described in detail above. The final volume of these micelles was adjusted to 10 mL.

Characterization studies

^1H NMR spectra of the block copolymers were recorded using a nuclear magnetic resonance spectrometer (Bruker ARX-300) with $CDCl_3$ or DMSO-d_6 as the solvent at room temperature. The prepared micelles were characterized by UV-vis absorption using a UV-2550 UV-visible spectrophotometer (Shimadzu, Japan) in the spectral range from 300 to 800 nm. Fluorescence spectra were recorded on a Hitachi F-4600 fluorescence spectrophotometer (Japan). Dynamic light scattering (DLS) experiments were performed on a laser light scattering spectrometer (BI-200SM) equipped with a digital correlator (BI-9000AT) at 636 nm. The zeta potentials of the aqueous polymer micelles were recorded with a Brookhaven ZetaPALS system (Brookhaven Instrument, USA). Transmission electron microscopy (TEM) images were obtained using a commercial Philips T20ST electron microscope at an acceleration voltage of 100 kV.

ROS detection

9,10-Anthracenediyl-bis(methylene) dimalonic acid (ABDA) was chosen as a probe to detect the generated singlet oxygen because ABDA can react rapidly with the anthracene moiety to effectively trap reactive oxygen species. PM, PM@Ag, PM@PpIX, and PM@PpIX@Ag (0.4 mg mL^{-1}) were mixed with ABDA (50 μM) dissolved in DMSO and activated by a 635 nm laser (power density of 0.25 W cm^{-2}) to monitor the ability of ROS production by measuring the absorption decrease of ABDA at 401 nm.

In vitro antibacterial activity

A single colony of bioluminescent *S. aureus* Xen36 cultured on agar plates was added into 10 mL tryptone soy broth (TSB) with 200 μg mL^{-1} kanamycin and incubated at 37 °C for 24 h during the preculture process. For the amplification culture of bacteria, the bacterial suspension was added in nineteen times the volume of TSB, followed by incubation for another 16 h. The final concentration of bacterial suspension was adjusted to meet the experimental requirements.

In order to determine the synergistic killing effect of micelles on bioluminescent *S. aureus* Xen36, 100 μL of PM, PM@PpIX, PM@Ag, and PM@PpIX@Ag with different concentrations (0, 12, 24, 50, 100, 200, 300 and 400 μg mL^{-1}) was

respectively added into 100 μL bacterial suspension (OD_{600} = 1, diluted with bacterial media), followed by incubation of 90 min at 37 °C. The treated solution was irradiated with a 635 nm laser for 10 min, using different micelles without light as the control group. The bactericidal efficacy of micelles was quantified by measuring the fluorescence intensity of suspensions with a bio-optical imaging system (PerkinElmer, IVIS Lumina II).

PM, PM@PpIX, PM@Ag, and PM@PpIX@Ag (400 μg mL^{-1}, 500 μL) were respectively added into 500 μL of bioluminescent *S. aureus* Xen36 suspension (OD_{600} = 10, diluted with bacterial media), followed by incubation for 90 min at 37 °C. The mixture was irradiated with a 635 nm laser for 10 min, and stained with calcein acetoxymethyl ester (Calcein-AM) (20 μM) and propidium iodide (PI) (5 μM) for 0.5 h at 37 °C in the dark. The fluorescence micrographs could be observed using a fluorescence microscope (Leica, DMI 6000B). The bacteria incubated with PBS, PM, PM@PpIX, PM@Ag, and PM@PpIX@Ag in the absence of laser activation were used as the control.

In vivo antibacterial study

According to the previous report of Shi,[30] murine skin infection models were established. BALB/c nude mice were subcutaneously injected with 100 μL of bioluminescent *S. aureus* Xen36 suspension (1×10^8 bacteria per mL) in the right side. The *S. aureus* Xen36 bearing-mice were photographed through a bio-optical imaging system (PerkinElmer, IVIS Lumina II) to measure the bioluminescence intensity. The murine skin infection model mice were randomly divided into 4 groups (6 mice per group) and subcutaneous injections of saline, PM@PpIX@Ag, PM@PpIX with laser activation and PM@PpIX@Ag with laser activation were administered near the infection sites every day (micelle concentration: 1 mg mL^{-1}). After five days of treatment, the skin tissues and the main organs of mice in different groups were obtained to conduct Gram staining assays and hematoxylin and eosin (H&E) staining, respectively.

Bacterial membrane integrity evaluation

The bacterial membrane potential test against bioluminescent *S. aureus* Xen36 was performed using a bacterial membrane potential kit (Thermo Fisher Scientific, BacLight™) containing the fluorescence dye 3,3′-diethyloxacarbocyanine iodide ($DiOC_2(3)$). $DiOC_2(3)$ at low concentrations could exhibit green fluorescence in bacterial cells and the self-association of the dye could cause the fluorescence emission to shift to red because of bacterial uptake. First, 1 mL of diluted bacterial suspension (OD_{600} = 1) was incubated with different micelles at the same concentration in 1.5 mL Eppendorf tubes at 37 °C for 4 h. Then, $DiOC_2(3)$ was added into the resultant mixture for another 15 min of incubation. Finally, the changes of relative fluorescence intensity were detected by flow cytometry (BD, Accuri C6). The bacterial suspension added into PBS solution without any polymeric micelles was used as a negative control, while bacterial suspension mixed with a membrane destroying reagent carbonyl cyanide 3-chlorophenylhydrazone (CCCP, 5 μM) was used as a positive control.

The integrity of bacterial membranes was evaluated by investigating the changes of bacterial morphologies before and after different treatments, using scanning electron microscopy (SEM). The samples for SEM analysis were prepared as follows. PM, PM@PpIX, PM@Ag, and PM@PpIX@Ag (400 μg mL^{-1}, 500 μL) were respectively added into 500 μL bacterial suspension (OD_{600} = 10), followed by incubation for 90 min at 37 °C. The mixture was irradiated with a 635 nm laser for 10 min. The bacteria mixed with PBS were used as a control. After centrifugation (5000 rpm, 5 min) and washing, the bacteria were tiled on the glass slides, fixed with 4% paraformaldehyde solution, dehydrated with a series of aqueous ethanol solutions (30%, 50%, 70%, 90%, and 100%), and dried at 25 °C. The SEM samples were required to be sprayed with gold before collecting SEM images.

Cell toxicity assay

For the MTT assay, NIH 3T3 cells were plated in 96-well plates at a density of 8×10^3 cells per well. After incubation of 24 h in a 5% CO_2 environment, cells were cultured in fresh medium containing with a graded concentration series of micelle solutions. Cells cultured in fresh medium without micelles were used as the control. Following a total of 24 h incubation at 37 °C, 20 μL of MTT solution (5 mg mL^{-1}) was added into each well. After incubation for another 4 h, the medium was removed and 150 μL of DMSO was added to dissolve the purple formazan. The optical absorption at 490 nm was immediately evaluated with a Varioskan Flash instrument (Thermo Scientific Company, USA). The cytotoxicity experiment was performed three times.

Hemolysis assay

For hemolysis assay, fresh rat blood cells were washed three times with sterile PBS buffer and harvested by centrifugation at 3000 rpm for 5 min. Then, 0.4 mL of diluted rat red blood cell suspension was incubated with 400 μL of different micelles at a predetermined concentration in 1.5 mL Eppendorf tubes at 37 °C for 4 h. The final solutions were centrifuged (3000 rpm, 5 min) and the ultraviolet absorptive value (570 nm) of the resultant supernatant (100 μL) was measured with a microplate reader. Rat red blood cell suspension mixed with PBS buffer without any polymeric micelles was used as a negative control, while rat red blood cell suspension mixed with Triton X-100 (0.1%) solution was used as a positive control. The hemolysis ratio (%) = (absorbance of experimental sample − absorbance of negative control sample)/(absorbance of positive control sample − absorbance of negative control sample) × 100.

Results and discussion

Preparation and characterization of polymeric antimicrobials

In this study, we first synthesized block copolymers PAsp-*b*-PCL *via* sequential ring-opening polymerization (ROP) of ε-CL

and BLA-NCA and facile removal of benzyl groups on the side chains; the chemical structure was confirmed with ^{1}H NMR as shown in Fig. S1A–C.† Then, after self-assembly in water, the PpIX-loaded polymeric micelles were fabricated from amphiphilic PAsp-*b*-PCL and hydrophobic PpIX and denoted as PM@PpIX. Finally, the silver nanoparticles were readily decorated on the surface of PM@PpIX through electrostatic adsorption of negatively charged PAsp shells for Ag^+ ions and the *in situ* reduction method; they were named PM@PpIX@Ag. Meanwhile, polymeric micelles based on only PAsp-*b*-PCL (PM) and micelles only modifying silver nanoparticles (PM@Ag) acted as the other controls except for PM@PpIX.

As seen in Fig. 1A, in comparison with the colorless PM, PM@PpIX displayed purplish-brown colour without any aggregates, suggesting that PpIX was successfully encapsulated into the PM and well dispersed in the aqueous solution. In contrast, the colors of PM@Ag and PM@PpIX@Ag were both dark brown and also no precipitation occurred, demonstrating the decoration of silver nanoparticles. The micelle sizes were measured by dynamic light scattering (DLS) and the result is presented in Fig. 1B. It was found that the average hydrodynamic diameter (D_h) of these micelles were all approximately 100–110 nm, in which PpIX encapsulation and silver decoration could give rise to a slight increase in size. The images of transmission electron microscopy (TEM) (Fig. 1C) showed that these micelles were all spherical in shape with diameters slightly smaller than that of DLS results, because of the dry state in TEM samples. The zeta potential (Fig. 1D) of PM was determined to be −55 ± 0.84 mV due to the carboxyl groups of the PAsp chains. Upon loading PpIX or decorating with silver nanoparticles, the zeta potentials of PM@PpIX and PM@Ag remarkably declined to −27 ± 0.98 mV and −31 ± 0.83 mV, respectively. By contrast, PM@PpIX@Ag exhibited the highest zeta potential with −17 ± 0.38 mV, indicating that the micelle

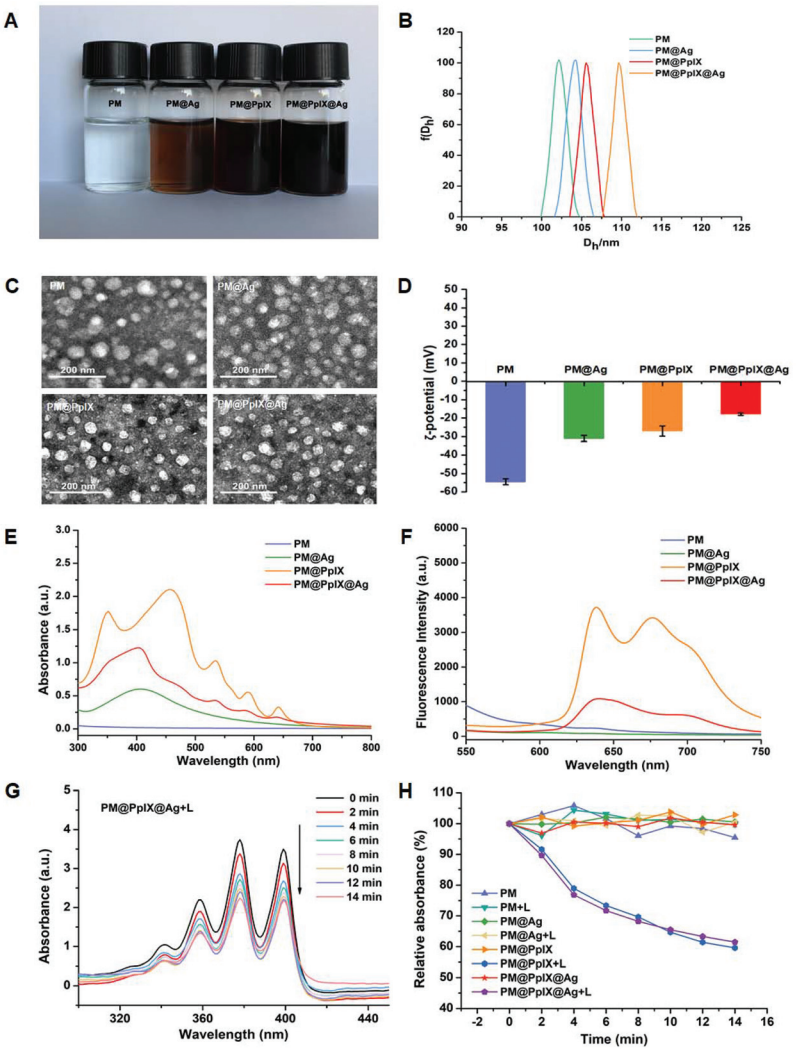

Fig. 1 (A) Photographs, (B) DLS measurement, (C) TEM images, (D) ζ-potentials, (E) UV–vis absorption spectra, and (F) fluorescence spectrum of different micelles (PM, PM@PpIX, PM@Ag and PM@PpIX@Ag). (G) UV–vis absorption spectra of ABDA detected the ROS production from PM@PpIX@Ag under laser activation for different times. (H) Relative absorption intensities of ABDA and four kinds of micelles with or without laser irradiation for various times. L means light activation.

was modified with silver nanoparticles and loaded PpIX concurrently. The UV-visible absorbance spectra of these micelles are displayed in Fig. 1E. PM displayed no obvious absorption peak, whereas PM@Ag and PM@PpIX exhibited characteristic peaks of nanosilver (around 400 nm) and protoporphyrin IX (Soret band and Q band[51,52]), which suggested that the micelles were successfully decorated with the silver nanoparticle and encased protoporphyrin IX, respectively. As for PM@PpIX@Ag, the absorption spectrum simultaneously displayed characteristic peaks of silver nanoparticles and PpIX, further confirming the successful integration of nanosilver and PpIX into a single entity by polymeric micelles. Fig. 1F shows the fluorescence spectra of these micelles. It was observed that PM@PpIX exhibited an emission peak at about 639 nm with a broad peak range from 658 nm to 750 nm under the excitation wavelength of 405 nm, while the fluorescence peak of PM@PpIX@Ag significantly declined compared with that of PM@PpIX, which was ascribed to strong resonant energy transfer from PpIX to the silver nanoparticles.[53]

To evaluate ROS generation capability of the fabricated micelles upon light activation, commercially available 9,10-anthracenediyl-bis(methylene)dimalonic acid (ABDA) was used as a probe for singlet oxygen ($^1O_2$). Upon exposure to laser irradiation, there was a substantial reduction of ABDA absorption at 401 nm in the presence of PM@PpIX@Ag, demonstrating that PM@PpIX@Ag could effectively produce $^1O_2$ content with a prolonged irradiation time (Fig. 1G). Moreover, the ROS generation efficiencies of PM@PpIX and PM@PpIX@Ag showed nearly no differences, suggesting that the decoration of silver nanoparticles would not discount the ROS-producing effect of PM@PpIX (Fig. 1H). In contrast, no obvious absorption decrease of ABDA was determined for the micelles without PpIX and groups in the absence of light irradiation. Meanwhile, the ROS response with lower concentrations of micelles is shown in Fig. S3.† The ROS generation ability of PM@PpIX@Ag and PM@PpIX gradually reduced with decreasing concentration, indicating that these two micelles produced $^1O_2$ in a concentration-dependent manner when the irradiation time was fixed. We then evaluated the ROS response in bacteria after incubation with different micelles and light exposure, utilizing DCFH-DA as a ROS probe. As presented in Fig. S4,† there was only weak green fluorescence in the fluorescence images of bacteria after treatment of PBS, PM, and PM@Ag under both dark and light conditions. In contrast, the PM@PpIX@Ag + L group and PM@PpIX + L group exhibited strong green fluorescence, further suggesting the ROS generation ability of PpIX-loaded micelles under light activation.

Chemo-photodynamic antibacterial effect of polymeric antimicrobials *in vitro*

To investigate the antibacterial activity of polymeric antimicrobials, *S. aureus* Xen36, a multi-drug-resistant bacterial strain with bioluminescence property,[30,54] was used as model bacteria. *S. aureus* Xen36 were incubated with different micelles and treated with or without irradiation, and the bioluminescence images were taken in which intensity was negatively correlated with antibacterial efficiency. As demonstrated in Fig. 2A and B, PM did not affect bacterial viability even under irradiation, while PM@Ag showed weak antibacterial

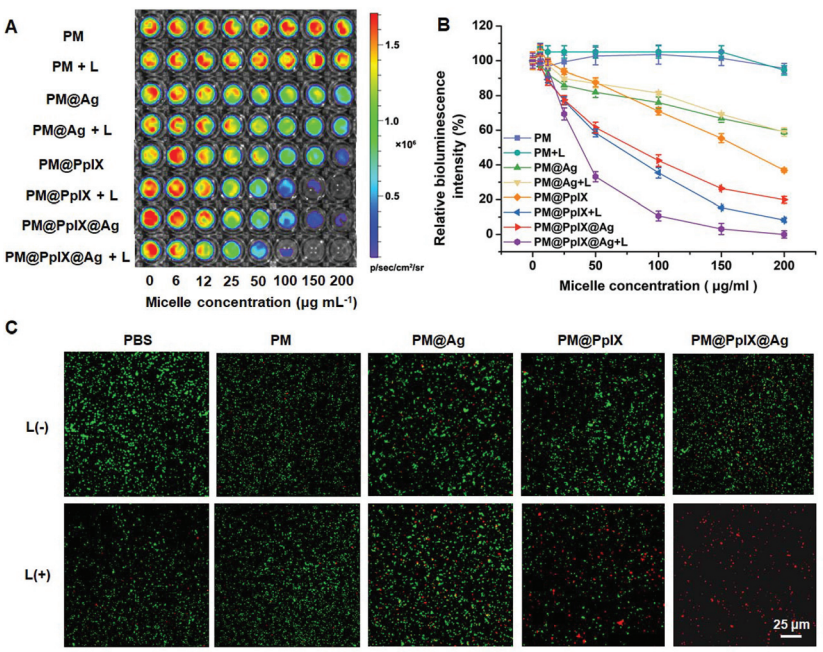

Fig. 2 Bioluminescence images (A) and relative bioluminescence intensities (B) of *S. aureus* Xen36 after being treated with PM, PM@PpIX, PM@Ag and PM@PpIX@Ag with different concentrations in both light and dark cases. (C) Fluorescence micrograph of *S. aureus* Xen36 after 1.5 h incubation with PBS, PM, PM@PpIX, PM@Ag and PM@PpIX@Ag in both the light and dark cases.

activity when its concentration reached 200 μg mL^{-1} regardless of irradiation, suggesting that decoration of silver nanoparticles could damage bacteria to some extent. However, the bioluminescence signal of the PM@PpIX group significantly decreased upon light activation, which indicated that PM@PpIX could kill *S. aureus* Xen36 through ROS generation. More importantly, PM@PpIX@Ag displayed improved antibacterial activity compared with PM@PpIX and PM@Ag, and the antibacterial effect could be observed at even lower concentrations, revealing that PM@PpIX@Ag could achieve a synergic effect in killing bacteria through PDT and silver nanoparticles.

To further confirm the synergistic antibacterial activity of the polymeric antimicrobials, we used a commercial LIVE/DEAD assay kit to detect the viability of bacteria after different treatments. The live bacteria could be stained by the dye Calcein-AM emitting green fluorescence while the dead bacteria were labeled with the red fluorescent dye PI. As shown in Fig. 2C, there was no notable red fluorescence in the fluorescence images of bacteria after treatment of PBS and PM under both dark and light conditions, signifying their negligible antibacterial activity. For PM@Ag, only sporadic red fluorescence could be observed regardless of light irradiation, which demonstrated that PM@Ag showed general toxicity towards bacteria and irradiation would not affect their antibacterial activity. However, the PM@PpIX group showed an increased red fluorescence upon irradiation, indicating their PDT antibacterial effect. Furthermore, the bacteria treated with the PM@PpIX@Ag + L group exhibited the strongest red fluorescence and no detectable green fluorescence was presented in the fluorescence image, suggesting that almost all the bacteria were killed and the PM@PpIX@Ag + L possessed the best antibacterial performance due to the excellent synergic chemo-photodynamic antibacterial effect.

Antibacterial activity of polymeric antimicrobials *in vivo*

Encouraged by the above results, we then assessed the bactericidal effect of the polymeric antimicrobials *in vivo* using the bioluminescent *S. aureus* Xen36-infected mouse model. The mice were divided into different four groups (PBS, PM@PpIX + L, PM@PpIX@Ag and PM@PpIX@Ag + L) and treated with the respective agents (Fig. 3A). The bioluminescence signal of the infection site was monitored for five consecutive days (Fig. 3B) and quantitative analysis of bioluminescence intensity and infected area are presented in Fig. 3C and D. The PBS group showed the slowest decrease of bioluminescent intensity and area and there was over 50% of infection at day 5 post-treatment. Compared with the PBS group, the mice treated with PM@PpIX + L and PM@PpIX@Ag showed faster reduction of bacterial bioluminescence but we could still observe approximately 20% of infection after 5 days of treatment. In contrast, PM@PpIX@Ag + L exhibited the strongest eradication effect on *S. aureus* Xen36 with almost no detectable bioluminescent intensity and area of infection. Subsequently, we photographed the infection site of mice on day 5 after treatment and performed Gram-staining to further evaluate the antibacterial efficacy. As shown in Fig. 3E, PM@PpIX@Ag + L showed the best healing property of the infection sites compared with those of the PBS group and other treatment groups. Moreover, almost no bacteria were observed in Gram-stained skin tissues for the PM@PpIX@Ag + L group and the histological structures were similar to that of healthy control. However, though there were fewer staphylococci compared to the PBS group, the PM@PpIX + L group and PM@PpIX@Ag group still appeared to have quiet a little of bacteria in the skin tissues. Therefore, these results revealed that the application of PM@PpIX@Ag + L exhibited the best bacteria-eradicating effect and infection-healing capability among those tested.

Antibacterial mechanism of polymeric antimicrobials

As demonstrated above, PM@PpIX@Ag showed excellent synergic chemo-photodynamic antibacterial effect in *in vitro* and *in vivo* testing. It has been widely established that the disruption of the bacterial membrane serves as a critical inducement of silver nanoparticles and PDT for bacterial death. We speculated that PM@PpIX@Ag could exert antibacterial effect by the destruction of the bacterial membrane, which follows a series of domino effects to cause bacterial death. To confirm the antibacterial mechanism of PM@PpIX@Ag, we detected the bacterial membrane potentials of *S. aureus* Xen36 after different treatments. As shown in Fig. 4A, the PM@PpIX@Ag + L group showed remarkably reduced red/green fluorescence ratios (0.21) compared with that of PM@PpIX@Ag (0.45) and PM@PpIX + L groups (0.35), indicating that the synergic chemo-photodynamic antibacterial effect could better disrupt the bacterial membrane integrity. We further probed the antibacterial mechanism of micelles by investigating the changes of bacterial morphologies before and after different treatments, using a scanning electron microscope. As shown in Fig. 4B, PBS-treated bacteria remained in their original morphology with intact round-shaped cell walls. In contrast, bacteria treated with different micelles displayed varying degrees of membrane lysis. Therein, bacteria in the PM@PpIX@Ag + L group exhibited severe damage where disrupted membranes fused together to produce the cell debris group. Collectively, the aforementioned results indicated that the synergic chemo-photodynamic effect of PM@PpIX@Ag obviously increased the capability of eliminating bacteria.

Biocompatibility assessment of polymeric antimicrobials

To evaluate the biocompatibility of our designed polymeric antimicrobials, the cytotoxicity of different micelles towards NIH3T3 cells was assessed by the MTT assay. As demonstrated in Fig. 5A, the cell viability of NIH3T3 cells treated with different micelles at predetermined concentrations was over 80%, indicating that these micelles exhibit excellent cytocompatibility for mammalian normal cells. Furthermore, we investigated the toxicity of these micelles to red blood cells through the hemolysis assay. As shown in Fig. 5B, there was no obvious hemolysis for all concentrations of these micelles and the hemolysis percentages of these micelles were within the scope of acceptable value even at a high concentration of 200 μg

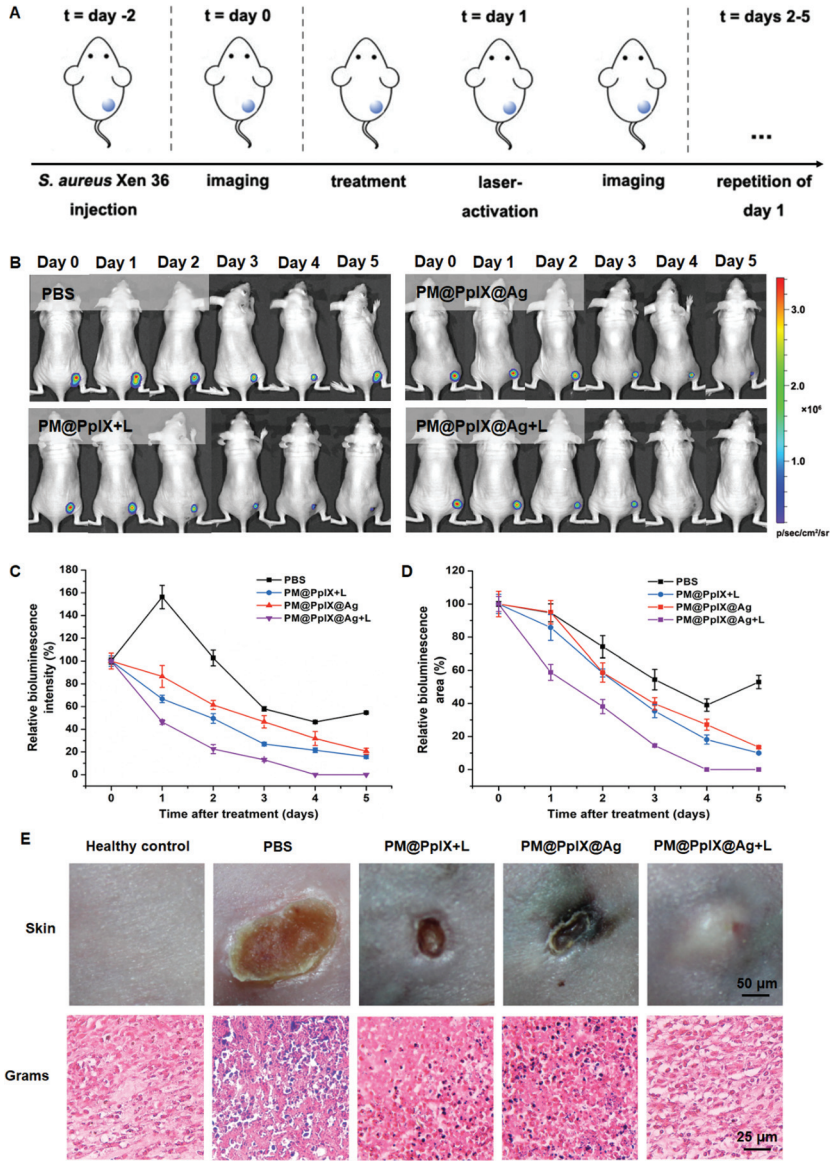

Fig. 3 (A) Workflow of bacterial infection, bio-optical imaging and treatment in mice. (B) Bioluminescence images of *S. aureus* Xen36-infected mice in the PBS, PM@PpIX@Ag, PM@PpIX + L, and PM@PpIX@Ag + L groups. (C) Relative bioluminescence intensities and (D) relative bioluminescent area of *S. aureus* Xen36-infected mice with different treatments. (E) Micrographs of the wound and Gram staining of skin tissues of infected mice with different treatments. The healthy mice were used as control.

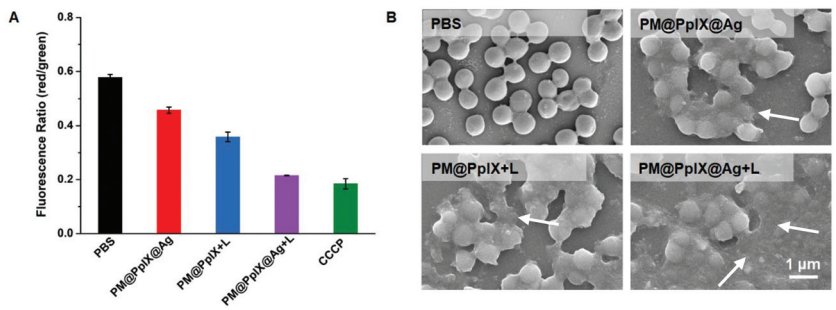

Fig. 4 (A) Membrane potential evaluation of *S. aureus* Xen36 after being treated with PBS, PM@PpIX@Ag, PM@PpIX + L, PM@PpIX@Ag + L and CCCP (positive control) by flow cytometry. (B) Morphology of *S. aureus* Xen36 after being treated with PBS, PM@PpIX@Ag, PM@PpIX + L, PM@PpIX@Ag + L using a scanning electron microscope.

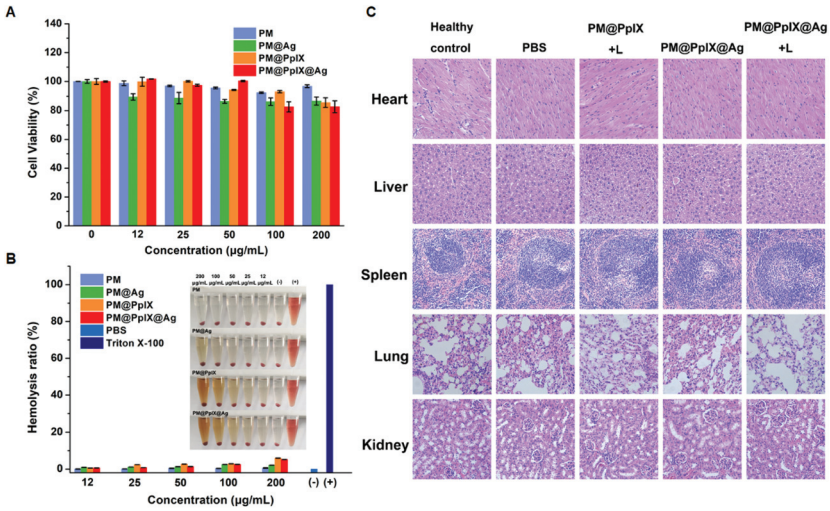

Fig. 5 (A) Cell cytotoxicity of NIH3T3 cells after treatment with PM, PM@Ag, PM@PpIX and PM@PpIX@Ag. (B) Hemolysis analysis of PM, PM@Ag, PM@PpIX and PM@PpIX@Ag at predetermined concentrations. Red blood cells incubated with PBS and 0.1% Triton X-100 (diluted with PBS) were used as negative (–) and positive (+) control, respectively. (C) H&E staining of main organs (spleen, lung, heart, liver, and kidney) of mice after 5 days of treatment from different groups.

mL^{-1}. In addition, the result of *in vivo* H&E analysis is shown in Fig. 5C. It was observed that the mice of all groups showed no signs of pathological changes in main organs. Moreover, we have compared the amount of Ag NPs available in the wound after 5 days and 10 days of treatment with PM@PpIX@Ag + Laser by ICP-MS analysis. As demonstrated in Table S3,† there were 6.36 μg Ag NPs in the wound after 5 days of treatment with PM@PpIX@Ag + Laser, and the Ag content decreased dramatically to 0.64 μg in the wound after 10 days of treatment with PM@PpIX@Ag + Laser, suggesting that the silver nanoparticles could be easily metabolized. Therefore, our polymeric antimicrobials had good potential to safely eradicate bacterial infections.

Conclusion

In summary, a silver-decorated, light-activatable polymeric antimicrobial with a strong synergistic effect was fabricated by us through a facile self-assembly strategy. Amphiphilic PAsp-*b*-PCL polymer micelles with negatively charged shells provide abundant binding sites for Ag ions which could be *in situ* reduced into silver nanoparticles, and the photosensitizer PpIX could be entrapped into the micellar core by hydrophobic interaction that could generate ROS upon light irradiation. The *in vitro* and *in vivo* experiments all proved that the antimicrobial performance of our combination system was superior to that of the other mono-therapy group, which benefited from the synergy of silver nanoparticle decoration and photodynamic eradication. The results of biosafety evaluation experiments confirmed that the obtained polymeric antimicrobial possessed negligible cytotoxicity to normal cells and long-term toxicity for the organism. Therefore, our work provides a feasible strategy to realize combined chemo-photodynamic therapy with enhanced potency for the treatment of bacterial infections.

Ethical statement

All animal procedures were performed in accordance with the Guidelines for the Care and Use of Laboratory Animals of Peking Union Medical College and experiments were approved by the Animal Experiments and Ethics Review Committee of the Institute of Radiation Medicine, Chinese Academy of Medical Sciences.

Conflicts of interest

There are no conflicts to declare.

Acknowledgements

This work was supported by the National Natural Science Foundation of China (No. 21708048 and 81722026), the Non-profit Central Research Institute Fund of Chinese Academy of Medical Sciences (2019-RC-HL-014 and 2018PT35031), the CAMS Innovation Fund for Medical Sciences (2016-I2M-3-022), the Drug Innovation Major Project (2018ZX09711-001-005), and the Fundamental Research Funds for the Central Universities (3332018194 and 3332018115).

References

1 H. K. Allen, J. Donato, H. H. Wang, K. A. Cloud-Hansen, J. Davies and J. Handelsman, Call of the wild: antibiotic re-

sistance genes in natural environments, *Nat. Rev. Microbiol.*, 2010, **8**, 251–259.
2 R. M. Klevens, M. A. Morrison, J. Nadle, S. Petit, K. Gershman, S. Ray, L. H. Harrison, R. Lynfield, G. Dumyati, J. M. Townes, A. S. Craig, E. R. Zell, G. E. Fosheim, L. K. McDougal, R. B. Carey and S. K. Fridkin, Invasive methicillin-resistant Staphylococcus aureus infections in the United States, *J. Am. Med. Assoc.*, 2007, **298**, 1763–1771.
3 C. Yang, C. Ren, J. Zhou, J. Liu, Y. Zhang, F. Huang, D. Ding, B. Xu and J. Liu, Dual fluorescent- and isotopic-labelled self-assembling vancomycin for in vivo, imaging of bacterial infections, *Angew. Chem., Int. Ed.*, 2017, **56**, 2356–2360.
4 D. Xu, W. Chen, Y. J. Tobin-Miyaji, C. R. Sturge, S. Yang, B. Elmore, A. Singh, C. Pybus, D. E. Greenberg, T. J. Sellati, W. Qiang and H. Dong, Fabrication and microscopic and spectroscopic characterization of cytocompatible self-assembling antimicrobial nanofibers, *ACS Infect. Dis.*, 2018, **4**, 1327–1335.
5 P. Courvalin, Predictable and unpredictable evolution of antibiotic resistance, *J. Intern. Med.*, 2008, **264**, 4–16.
6 F. Maechler, C. Geffers, F. Schwab, L.-A. Peña Diaz, M. Behnke and P. Gastmeier, Entwicklung der resistenzsituation in deutschland, *Med. Klin., Intensivmed. Notfallmed.*, 2017, **112**, 186–191.
7 F. Huang, Y. Gao, Y. Zhang, T. Cheng, H. Ou, L. Yang, J. Liu, L. Shi and J. Liu, Silver-decorated polymeric micelles combined with curcumin for enhanced antibacterial activity, *ACS Appl. Mater. Interfaces*, 2017, **9**, 16880–16889.
8 C. Yang, F. Hu, X. Zhang, X. Zhang, F. Huang, J. Liu, Y. Zhang, L. Yang, Y. Gao, B. Liu and J. Liu, Combating bacterial infection by in situ self-assembly of AIEgen-peptide conjugate, *Biomaterials*, 2020, **244**, 119972.
9 S. Tian, L. Su, Y. Liu, J. Cao, G. Yang, Y. Ren, F. Huang, J. Liu, Y. An, H. C. van der Mei, H. J. Busscher and L. Shi, Self-targeting, zwitterionic micellar dispersants enhance antibiotic killing of infectious biofilms-an intravital imaging study in mice, *Sci. Adv.*, 2020, **6**, eabb1112.
10 Y. Huang and H. Huang, Effects of clinical dental implant abutment materials and their surface characteristics on initial bacterial adhesion, *Rare Met.*, 2019, **38**, 512–519.
11 J. Li, X. Liu, L. Tan, Z. Cui, X. Yang, Y. Liang, Z. Li, S. Zhu, Y. Zheng, K. W. K. Yeung, X. Wang and S. Wu, Zinc-doped prussian blue enhances photothermal clearance of Staphylococcus aureus and promotes tissue repair in infected wounds, *Nat. Commun.*, 2019, **10**, 4490.
12 J. Li, X. Liu, Z. Zhou, L. Tan, X. Wang, Y. Zheng, Y. Han, D. Chen, K. W. K. Yeung, Z. Cui, X. Yang, Y. Liang, Z. Li, S. Zhu and S. Wu, Lysozyme-assisted photothermal eradication of methicillin-resistant Staphylococcus aureus infection and accelerated tissue repair with natural melanosome nanostructures, *ACS Nano*, 2019, **13**, 11153–11167.
13 M. Li, L. Li, K. Su, X. Liu, T. Zhang, Y. Liang, D. Jing, X. Yang, D. Zheng, Z. Cui, Z. Li, S. Zhu, K. W. K. Yeung, Y. F. Zheng, X. Wang and S. Wu, Highly effective and non-invasive near–infrared eradication of a Staphylococcus aureus biofilm on implants by a photoresponsive coating within 20 Min, *Adv. Sci.*, 2019, **6**, 1900599.
14 Y. Luo, J. Li, X. Liu, L. Tan, Z. Cui, X. Feng, X. Yang, Y. Liang, Z. Li, S. Zhu, Y. Zheng, K. W. K. Yeung, C. Yang, X. Wang and S. Wu, Dual metal–organic framework heterointerface, *ACS Cent. Sci.*, 2019, **5**, 1591–1601.
15 X. Xie, C. Mao, X. Liu, Y. Zhang, Z. Cui, X. Yang, K. W. K. Yeung, H. Pan, P. K. Chu and S. Wu, Synergistic bacteria killing through photodynamic and physical actions of graphene oxide/Ag/collagen coating, *ACS Appl. Mater. Interfaces*, 2017, **9**, 26417–26428.
16 S. Li, S. Cui, D. Yin, Q. Zhu, Y. Ma, Z. Qian and Y. Gu, Dual antibacterial activities of a chitosan-modified upconversion photodynamic therapy system against drug-resistant bacteria in deep tissue, *Nanoscale*, 2017, **9**, 3912–3924.
17 E. Gholibegloo, A. Karbasi, M. Pourhajibagher, N. Chiniforush, A. Ramazani, T. Akbari, A. Bahador and M. Khoobi, Carnosine-graphene oxide conjugates decorated with hydroxyapatite as promising nanocarrier for ICG loading with enhanced antibacterial effects in photodynamic therapy against Streptococcus mutans, *J. Photochem. Photobiol., B*, 2018, **181**, 14–22.
18 C. Mao, Y. Xiang, X. Liu, X. Yang, Z. Li, S. Zhu, Y. Zheng, K. W. K. Yeung and S. Wu, Repeatable photodynamic therapy with triggered signaling pathways of fibroblast cell proliferation and differentiation to promote bacteria-accompanied wound healing, *ACS Nano*, 2018, **12**, 1747–1759.
19 K. Pu, A. J. Shuhendler and J. Rao, Semiconducting polymer nanoprobe for in vivo imaging of reactive oxygen and nitrogen species, *Angew. Chem., Int. Ed.*, 2013, **52**, 10325–10329.
20 Z. Zhou, J. Song, L. Nie and X. Chen, Reactive oxygen species generating systems meeting challenges of photodynamic cancer therapy, *Chem. Soc. Rev.*, 2016, **23**, 6597–6626.
21 S. L. H. Higgins and K. J. Brewer, Designing red-light-activated multifunctional agents for the photodynamic therapy, *Angew. Chem., Int. Ed.*, 2012, **51**, 11420–11422.
22 A. Felgentrager, T. Maisch, A. Spath, J. A. Schroder and W. Baumler, Singlet oxygen generation in porphyrin-doped polymeric surface coating enables antimicrobial effects on Staphylococcus aureus, *Phys. Chem. Chem. Phys.*, 2014, **16**, 20598–20607.
23 C. L. Campbell, C. T. A. Brown, K. Wood, A. G. Salvio, N. M. Inada, V. S. Bagnato and H. Moseley, A quantitative study of in vivo protoporphyrin IX fluorescence build up during occlusive treatment phases, *Photodiagn. Photodyn. Ther.*, 2017, **18**, 204–207.
24 G. Zampini, L. Tarpani, G. Massaro, M. Gambucci, A. Nicoziani and L. Latterini, Effects of gold colloids on the photosensitization efficiency of silica particles doped with protoporphyrin IX, *ChemPhotoChem*, 2017, **1**, 553–561.
25 L. Yan, J. Miller, M. Yuan, J. F. Liu, T. M. Busch, A. Tsourkas and Z. Cheng, Improved photodynamic

therapy efficacy of protoporphyrin IX-loaded polymeric micelles using erlotinib pretreatment, *Biomacromolecules*, 2017, **6**, 1836–1844.

26 H. Eshghi, A. Hossein, M. Sazgarnia, N. Ameneh, M. Rahimizadeh and S. Mohammad, Protoporphyrin IX–gold nanoparticle conjugates as an efficient photosensitizer in cervical cancer therapy, *Photodiagn. Photodyn. Ther.*, 2013, **10**, 304–312.

27 G. Zampini, O. Planas, F. Marmottini, O. Gulias, M. Agut, S. Nonell and L. Latterini, Morphology effects on singlet oxygen production and bacterial photoinactivation efficiency by different silica-protoporphyrin IX nanocomposites, *RSC Adv.*, 2017, **7**, 14422–14429.

28 D. Wang, L. Zhu, Y. Pu, J.-X. Wang, J.-F. Chen and L. Dai, Transferrin-coated magnetic upconversion nanoparticles for efficient photodynamic therapy with near-infrared irradiation and luminescence bioimaging, *Nanoscale*, 2017, **31**, 11214–11221.

29 N. Zhang, F. Zhao, Q. Zou, Y. Li, G. Ma and X. Yan, Multitriggered tumor-responsive drug delivery vehicles based on protein and polypeptide coassembly for enhanced photodynamic tumor ablation, *Small*, 2016, **43**, 5936–5943.

30 Y. Liu, H. C. van der Mei, B. Zhao, Y. Zhai, T. Cheng, Y. Li, Z. Zhang, H. J. Busscher, Y. Ren and L. Shi, Eradication of multidrug-resistant Staphylococcal infections by light-activatable micellar nanocarriers in a murine model, *Adv. Funct. Mater.*, 2017, **27**, 1701974.

31 P. D. Tamma, S. E. Cosgrove and L. L. Maragakis, Combination therapy for treatment of infections with gram-negative bacteria, *Clin. Microbiol. Rev.*, 2012, **25**, 450–470.

32 J. W. Betts, A. S. Sharili, R. M. La Ragione and D. W. Wareham, In vitro antibacterial activity of curcumin–polymyxin B combinations against multidrug-resistant bacteria associated with traumatic wound infections, *J. Nat. Prod.*, 2016, **79**, 1702–1706.

33 J. Zhang, Y. Sun, Y. Zhao, Y. Liu, X. Yao, B. Tang and R. Hang, Antibacterial ability and cytocompatibility of Cu-incorporated Ni–Ti–O nanopores on NiTi alloy, *Rare Met.*, 2019, **38**, 552–560.

34 E. Zhang, S. Fu, R. Wang, H. Li, Y. Liu, Z. Ma, G. Liu, C. Zhu, G. Qin and D. Chen, Role of Cu element in biomedical metal alloy design, *Rare Met.*, 2019, **38**, 476–494.

35 B. Huang, X. Liu, L. Tan, Z. Cui, X. Yang, D. Jing, D. Zheng, Z. Li, Y. Liang, S. Zhu, K. W. K. Yeung, X. Wang, Y. Zheng and S. Wu, "Imitative" click chemistry to form a sticking xerogel for the portable therapy of bacteria-infected wounds, *Biomater. Sci.*, 2019, **7**, 5383–5387.

36 N. Hao, K. W. Jayawardana, X. Chen and M. Yan, One-step synthesis of amine-functionalized hollow mesoporous silica nanoparticles as efficient antibacterial and anticancer materials, *ACS Appl. Mater. Interfaces*, 2015, **7**, 1040–1045.

37 X. Dai, Q. Guo, Y. Zhao, P. Zhang, T. Zhang, X. Zhang and C. Li, Functional silver nanoparticle as a benign antimicrobial agent that eradicates antibiotic-resistant bacteria and promotes wound healing, *ACS Appl. Mater. Interfaces*, 2016, **8**, 25798–25807.

38 M. Qasim, N. Udomluck, J. Chang, H. Park and K. Kim, Antimicrobial activity of silver nanoparticles encapsulated in poly-N-isopropylacrylamide-based polymeric nanoparticles, *Int. J. Nanomed.*, 2018, **13**, 235–249.

39 F. Porcaro, L. Carlini, A. Ugolini, D. Visaggio, P. Visca, I. Fratoddi, I. Venditti, C. Meneghini, L. Simonelli and C. Marini, Synthesis and structural characterization of silver nanoparticles stabilized with 3-mercapto-1-propansulfonate and 1-thioglucose mixed thiols for antibacterial applications, *Materials*, 2016, **9**, 1028–1042.

40 J. Chen, F. Wang, Q. Liu and J. Du, Antibacterial polymeric nanostructures for biomedical applications, *Chem. Commun.*, 2014, **50**, 14482–14493.

41 K. Mijnendonckx, N. Leys, J. Mahillon, S. Silver and R. Van Houdt, Antimicrobial silver: uses, toxicity and potential for resistance, *BioMetals*, 2013, **26**, 609–621.

42 O. Lyutakov, O. Hejna, A. Solovyev, Y. Kalachyova and V. Svorcik, Polymethylmethacrylate doped with porphyrin and silver nanoparticles as light-activated antimicrobial material, *RSC Adv.*, 2014, **4**, 50624–50630.

43 Y. Zhang, P. Sun, L. Zhang, Z. Wang, F. Wang, K. Dong, Z. Liu, J. Ren and X. Qu, Silver–infused porphyrinic metal–organic framework: surface–adaptive, on–demand nanoplatform for synergistic bacteria killing and wound disinfection, *Adv. Funct. Mater.*, 2019, 1808594.

44 I. Venditti, G. Testa, F. Sciubba, L. Carlini, F. Porcaro, C. Meneghini, S. Mobilio, C. Battocchio and I. Fratoddi, Hydrophilic metal nanoparticles functionalized by 2-Diethylaminoethanethiol: a close look at the metal–ligand interaction and interface chemical structure, *J. Phys. Chem. C*, 2017, **121**, 8002–8013.

45 F. Mochi, L. Burratti, I. Fratoddi, I. Venditti, C. Battocchio, L. Carlini, G. Iucci, M. Casalboni, F. De Matteis and S. Casciardi, Plasmonic sensor based on interaction between silver nanoparticles and Ni2+ or Co2+ in water, *Nanomaterials*, 2018, **8**, 488–501.

46 Y. Xu, S. Li and P. Chang, A facile method to produce silver nanoparticle-loaded regenerated cellulose membranes via the reduction of silver nitrate in a homogeneous system, *BioResources*, 2017, **12**, 9050–9062.

47 Y. Wang, J. Wan, R. J. Miron, Y. Zhao and Y. Zhang, Antibacterial properties and mechanisms of gold–silver nanocages, *Nanoscale*, 2016, **8**, 11143–11152.

48 J. Gagnon, M. J. D. Clift, D. Vanhecke, I. Widnersson, S. L. Abram, A. Fink, R. Caruso, B. Rothen and K. Fromm, Synthesis, characterization, antibacterial activity and cytotoxicity of hollow TiO2-coated CeO2 nanocontainers encapsulating silver nanoparticles for controlled silver release, *J. Mater. Chem. B*, 2016, **4**, 1166–1174.

49 B. Jiang, Q. Wu, L. Zhang and Y. Zhang, Preparation and application of silver nanoparticle-functionalized magnetic graphene oxide nanocomposites, *Nanoscale*, 2017, **9**, 1607–1615.

50 J. Chen, F. Wang, Q. Liu and J. Du, Antibacterial polymeric nanostructures for biomedical applications, *Chem. Commun.*, 2015, **46**, 14482–14493.
51 R. Giovannetti, *The use of spectrophotometry UV-Vis for the study of porphyrins. macro to nano spectroscopy*, InTech, 2012, pp. 87–108.
52 L. Ning, P. Liu, B. Wang, C. Li, E. Kang, Z. Lu, X. Hu and L. Xu, Hydrothermal derived protoporphyrin IX nanoparticles for inactivation and imaging of bacteria strains, *J. Colloid Interface Sci.*, 2019, **549**, 72–79.
53 F. Hu, C. Li, Y. Zhang, M. Wang, D. Wu and Q. Wang, Real-time in vivo, visualization of tumor therapy by a near-infrared-II Ag2S quantum dot-based theranostic nanoplatform, *Nano Res.*, 2015, **8**, 1637–1647.
54 Y. Liu, H. J. Busscher, B. Zhao, Y. Li, Z. Zhang, H. C. van der Mei, Y. Ren and L. Shi, Surface-adaptive, antimicrobially loaded, micellar nanocarriers with enhanced penetration and killing efficiency in staphylococcal biofilms, *ACS Nano*, 2016, **10**, 4779–4789.